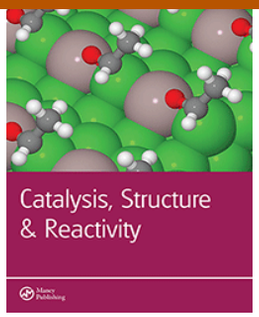

Catalysis, Structure & Reactivity

ISSN: 2055-074X (Print) 2055-0758 (Online) Journal homepage: http://www.tandfonline.com/loi/ycsr20

Production of Butylamine in the Gas Phase Hydrogenation of Butyronitrile over Pd/SiO_2 and $Ba\text{-}Pd/SiO_2$

Y. Hao, M. Li, F. Cárdenas-Lizana & M. A. Keane

To cite this article: Y. Hao, M. Li, F. Cárdenas-Lizana & M. A. Keane (2015) Production of Butylamine in the Gas Phase Hydrogenation of Butyronitrile over Pd/SiO_2 and $Ba\text{-}Pd/SiO_2$, Catalysis, Structure & Reactivity, 1:3, 132-139, DOI: 10.1179/2055075815Y.0000000007

To link to this article: http://dx.doi.org/10.1179/2055075815Y.0000000007

Catalysis, Structure & Reactivity

Original Research Paper

Production of butylamine in the gas phase hydrogenation of butyronitrile over Pd/SiO_2 and $Ba\text{-}Pd/SiO_2$

Y. Hao, M. Li, F. Cárdenas-Lizana and M. A. Keane*

Chemical Engineering, School of Engineering and Physical Sciences, Heriot-Watt University, Edinburgh EH14 4AS, Scotland

Abstract The gas phase (1 atm, 473–563 K) hydrogenation of butyronitrile has been studied over Pd/SiO_2 and $Ba–Pd/SiO_2$. Catalysts characterization involved temperature-programmed reduction (TPR), H_2/NH_3 chemisorption/temperature programmed desorption (TPD), X-ray diffraction (XRD), and TEM measurements. The incorporation of Ba with Pd resulted in the formation of smaller metal nano-particles (7 vs 28 nm) with a resultant (seven-fold) higher H_2 chemisorption and decreased total surface acidity (from NH_3 chemisorption/TPD). Temperature-related activity maxima were observed for both catalysts and are associated with thermal desorption of the nitrile reactant. Exclusivity to the target butylamine was achieved at $T \geq 543$ K where $Ba–Pd/SiO_2$ delivered higher selective hydrogenation rate (91 mol h^{-1} mol_{Pd}^{-1}) than Pd/SiO_2 (54 mol h^{-1} mol_{Pd}^{-1}), attributed to greater availability of surface-reactive hydrogen. Lower surface acidity served to minimize condensation to higher amines. The rate and selectivity to butylamine exceed those previously reported for gas phase operation.

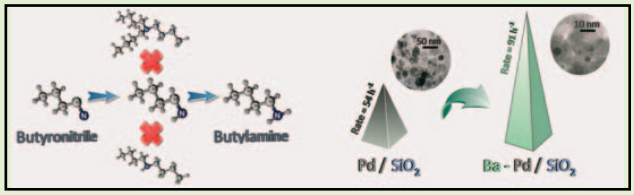

Keywords Selective hydrogenation, Butyronitrile, Butylamine, Pd/SiO_2, $Ba–Pd/SiO_2$

Cite this article Y. Hao, M. Li, F. Cárdenas-Lizana and M. A. Keane. *Catal. Struct. React.*, 2015, 1, 132-139

Introduction

Primary aliphatic amines are widely used in the textile, pharmaceutical, fine chemical, and agrochemical sectors.[1] Industrial amine production is based on nitrile hydrogenation where undesired formation of secondary and tertiary amines is difficult to avoid.[1,2] Taking the hydrogenation of butyronitrile (Fig. 1), partial reduction (step (I)) generates an imine (butylidenimine) as reactive intermediate that is converted (step (II)) to the target butylamine. The latter can participate in a condensation (step (III)) with the imine and reduction (step (IV)) to produce the secondary amine (dibutylamine) with NH_3 elimination. Additional condensation of dibutylamine and imine (step (V)) and subsequent hydrogenation (step (VI)) generate the tertiary amine (tributylamine).[3] Nitrile hydrogenation has been predominantly conducted in batch liquid phase at elevated H_2 pressures (20–45 bar).[4–8] A range of supported transition metal (Ru,[5,9] Ni,[4,10–12] Co,[8,13,14] Rh,[5] Cu,[6] Pd,[5,15] and Pt[5,15]) catalysts has been used, where Ru, Ni, and Co favored primary amine formation, Rh and Cu generated the secondary amine, and Pd and Pt promoted amine mixtures.[2] There is evidence that reaction rate is dependent on the catalytic metal where the following sequence of decreasing activity has been reported in batch liquid phase hydrogenation of butyronitrile over SiO_2 supported catalysts:[16] Ni > Co > Pt > Ru > Cu > Pd. A move from batch to continuous processes has been highlighted by the fine chemical industry as a priority to reduce downtime and increase throughput.[17] Supported Ni catalysts have been applied in gas phase operation but low selectivity to the target primary amine and loss of activity with time on-stream are decided drawbacks.[10,11,18–21] Use of Pd/ZnO has delivered high selectivity (99%) to ethylamine but low activity (conversions <6%) in acetonitrile conversion where (PdZn) alloy formation served to inhibit condensation to higher amines.[22]

Selectivity in nitrile reduction is affected by the acid–base properties of the support[4] and electronic character of the metal site[23] which, in turn, is influenced by the use of additives and/or promoters.[24] An increase in carrier basicity (by nitrogen doping[10] or LiOH treatment[13]) inhibits condensation in the hydrogenation of butyronitrile (Fig. 1, steps (III) and (V)). Moreover, use of ammonia provides a basic reaction medium that can enhance primary amine selectivity.[2] Modifications to the electron density

*Corresponding author, email m.a.keane@hw.ac.uk

Received 10 June 2015; accepted 20 July 2015
DOI 10.1179/2055075815Y.0000000007

Maney Publishing

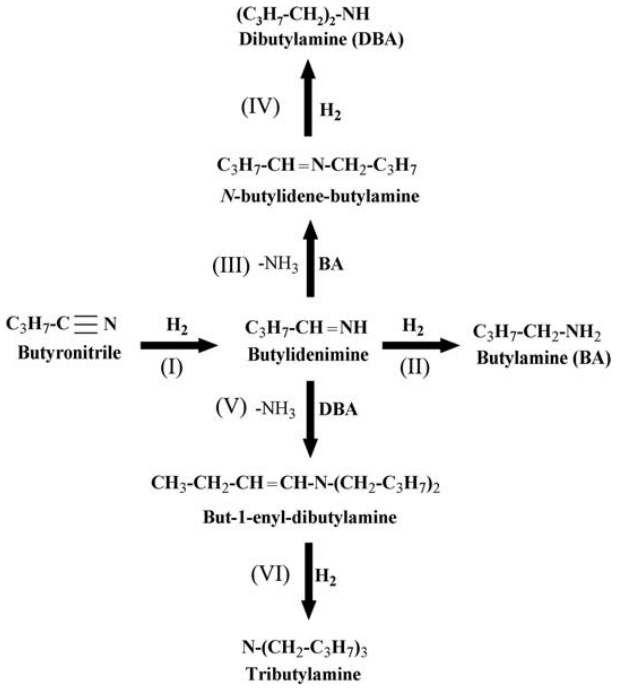

Figure 1 Reaction scheme for the hydrogenation of butyronitrile

of supported metal sites can also impact on product distribution where the formation of negatively charged (Cu) nanoparticles was deemed essential for the selective synthesis of *n*-propylamine.[24] Although supported nano-scale Pd has been widely adopted in catalytic hydrogenation,[25,26] application in nitrile conversion is limited. This is most likely due to the observed low activity and selectivity to primary amines.[2,7,15,16] In previous work, we reported the formation of a supported $Pd^{\delta-}$ phase on Ba–Pd/SiO_2 with greater H_2 uptake capacity relative to Pd/SiO_2.[27] Authors explore here the promoting effect of Ba in Pd/SiO_2 as an approach to enhanced butylamine production in gas phase butyronitrile hydrogenation.

Experimental

Catalyst preparation, activation, and characterization

A 5% w/w Pd/SiO_2 was prepared by impregnation of fumed SiO_2 (Aldrich) with $Pd(OAc)_2$ in dimethylformamide (DMF). The DMF was removed from the impregnated sample under vacuum over 12 h at ambient temperature. The Ba–Pd complex ($(DMF)_xBaPd(CN)_4)_\infty$ bimetallic precursor was prepared as described elsewhere.[28] The SiO_2 support was added to a solution of the precursor in DMF to deliver a 5% w/w Pd loading (Pd/Ba = 1 mol mol^{-1}). Samples were sieved (ATM fine test sieves) into batches of 75 μm mean particle diameter and activated by reduction in flowing (60 cm^3 min^{-1}) dry H_2 (BOC, 99.99%) at 10 K min^{-1} to 573 K, flushed in N_2/He, cooled to ambient temperature, and passivated in 1% v/v O_2/He for *ex situ* analysis. Metal loading was determined by inductively coupled plasma-optical emission spectrometry (ICP-OES, Vista-PRO, Varian Inc. (Palo Alto, USA)) from the diluted extract of aqua regia (25% v/v HNO_3/HCl). Nitrogen adsorption/desorption, temperature programmed reduction (TPR), H_2 (and NH_3) chemisorption, and temperature-programmed desorption (TPD) were performed using the commercial CHEM-BET 3000 (Quantachrome) unit equipped with an on-line thermal conductivity detector (TCD) and data acquisition using the TPR Win™ software. Samples (0.05–0.1 g) were loaded in a U-shaped Quartz cell (3.76 mm *i.d.*), outgassed for 30 min, and the total specific surface area (SSA) recorded in a 30% v/v N_2/He flow with undiluted N_2 (BOC, 99.9%) as internal standard. Two cycles of N_2 adsorption–desorption were employed using the standard single-point BET method. Temperature-programmed reduction analysis was conducted in 17 cm^3 min^{-1} (Brooks mass flow controlled) 5% v/v H_2/N_2 at 10 K min^{-1} to 573 K. The reduced sample was maintained at 573 K in H_2/N_2 until the signal returned to baseline, swept with 65 cm^3 min^{-1} N_2/He for 1.5 h, cooled to ambient temperature, and subjected to an undiluted H_2 (BOC, 99.99%) or NH_3 (BOC, 99.98%) pulse (50–1000 μL) titration procedure. A contribution due to Pd hydride formation can be discounted as H_2 partial pressure (<2 torr) in the sample cell was well below that (>11 torr) required to generate the hydride.[29] Samples were thoroughly flushed in N_2/He (65 cm^3 min^{-1}) to remove weakly bound H_2 (or NH_3) and subjected to TPD (at 10–50 K min^{-1}) to 1000–1273 K with a final isothermal hold until the signal returned to baseline. The resultant profile was corrected using the TPD recorded in parallel directly following TPR to explicitly determine H_2 (or NH_3) release. Powder X-ray diffraction (XRD) analyses were conducted on a Bruker/Siemens D500 incident X-ray diffractometer using Cu Kα radiation; samples were scanned at 0.02° $step^{-1}$ over the range $20° \leq 2\theta \leq 90°$. Diffractograms were identified using JCPDS-ICDD reference standards (Pd (05-0681) and $BaSiO_3$ (04-0504)). Palladium particle size was obtained from the Scherrer equation,[30]

$$d_c = \frac{K\lambda}{\beta \cos\theta} \quad (1)$$

where d_c is the mean size of the ordered (crystalline) domains, K is a dimensionless shape factor (0.9), λ the X-ray wavelength (1.5056 Å), β line broadening at half the maximum intensity, and θ the Bragg angle ($2\theta = 40.1°$). Palladium particle morphology (size and shape) was determined by transmission electron microscopy analysis, conducted on a JEOL-2000 TEM/STEM microscope equipped with a UTW energy dispersive X-ray (EDX) detector (Oxford Instruments), and operated at an accelerating voltage of 200 kV. Samples were prepared by ultrasonic dispersion in 2-butanol, evaporating a drop of the resultant suspension onto a holey carbon/Cu grid (300 mesh). Up to 800 individual particles were counted for each catalyst and the mean metal diameter (d_{TEM}) calculated from

$$d_{TEM} = \frac{\sum_i n_i d_i}{\sum_i n_i} \quad (2)$$

where n_i is the number of particles of diameter d_i.

Hydrogenation of butyronitrile

Catalytic system

The hydrogenation of butyronitrile (Sigma-Aldrich, ≥99%) was conducted *in situ* following catalyst activation at 1 atm and 473–563 K in a fixed bed vertical glass reactor

(*i.d.* = 15 mm). Reactions were conducted under operating conditions that ensured negligible internal or external mass and heat transfer limitations. The nitrile reactant was delivered at a fixed calibrated flowrate (0.6 $cm^3 h^{-1}$) via a glass/teflon air-tight syringe and teflon line using a microprocessor controlled infusion pump (Model 100 kDa Scientific). A layer of borosilicate glass beads served as preheating zone, ensuring that the reactant was vaporized and reached reaction temperature before contacting the catalyst. Isothermal conditions (±1 K) were maintained by diluting the catalyst bed with ground glass (75 μm); the ground glass was mixed thoroughly with the catalyst before insertion in the reactor. Reaction temperature was continuously monitored using a thermocouple inserted in a thermowell within the catalyst bed. A co-current flow of butyronitrile and H_2 (<1% volume by volume nitrile in H_2) was maintained at GHSV = $1.0 \times 10^4 h^{-1}$. The inlet nitrile flow (F) was constant (6.9 mmol h^{-1}) where the H_2 content was in excess (by a factor of 12 relative to the stoichiometric requirement for butylamine formation) and monitored using a Humonics (Model 520) digital flowmeter. Molar palladium (n) to F ratio spanned the range 3.4×10^{-4}–3.4×10^{-3} h. The reactor effluent was frozen in a liquid N_2 trap for subsequent analysis, which was made using a Perkin-Elmer Auto System XL chromatograph equipped with a programed split/splitless injector and a flame ionization detector, employing a DB-1 capillary column (*i. d.* = 0.33 mm, length = 50 m, film thickness = 0.20 μm). Data acquisition and manipulation were performed using the TurboChrom Workstation Version 6.1.2 (for Windows) chromatography data system. Fractional butyronitrile conversion (X) was obtained from

$$X = \frac{[\text{Butyronitrile}]_{in} - [\text{Butyronitrile}]_{out}}{[\text{Butyronitrile}]_{in}} \quad (3)$$

and nitrile consumption rate from

$$\text{Rate}\,(h^{-1}) = \frac{X \times F}{n} \quad (4)$$

where selectivity to product "*i*" (S_i) is given by

$$S_i(\%) = \frac{N_i x_i}{\sum N_i x_i} \times 100 \quad (5)$$

$[\text{Butyronitrile}]_{in}$ and $[\text{Butyronitrile}]_{out}$ represent inlet and outlet concentration, respectively, and N_i is the stoichiometric coefficient for product [a]*i*. In blank tests, passage of butyronitrile in a stream of H_2 through the empty reactor or over the SiO_2 support alone did not result in any detectable conversion. Repeated reactions with different samples of catalyst from the same batch delivered raw data reproducibility and carbon mass balance better than ±6%.

Thermodynamic analysis

Application of thermodynamics provides an important guide to the maximum conversion/selectivity possible under a given set of reaction conditions. Butyronitrile, hydrogen, and all products (butylamine, dibutylamine, tributylamine, and NH_3) were considered. Setting the inlet nitrile at 1 mol, product distribution at equilibrium was determined over 473–563 K at a total pressure of 1 atm, where the H_2/butyronitrile molar ratio was kept constant (= 24) to mimic catalytic reaction conditions. Equilibrium calculations were made using CHEMCAD (Version 6) where the Gibbs reactor facility was applied to obtain product composition under conditions of minimized Gibbs free energy. The equation of state for fugacity employed the Soave–Redlich–Kwong approach.[31] The total Gibbs function is given by

$$G^t = \sum_{i=1}^{N} n_i \bar{G}_i = \sum_{i=1}^{N} n_i \bar{\mu}_i = \sum n_i G_i^0 + RT \sum n_i \ln \frac{\hat{f}_i}{f_i^0} \quad (6)$$

For gas phase reaction equilibrium, $\hat{f}_i = \hat{\phi}_i y_i P$, $f_i^0 = P^0$ and $\Delta G^0 = \Delta G_{f_i}^0$ and the minimum Gibbs free energy of each gaseous species and total for the system can be expressed by

$$\Delta G_{f_i}^0 + RT \ln \frac{\hat{\phi}_i y_i P}{P^0} + \sum_k \lambda_k a_{ik} = 0 \quad (7)$$

$$\sum_{i=1}^{N} n_i \left(\Delta G_{f_i}^0 + RT \ln \frac{\hat{\phi} y_i P}{P^0} + \sum_k \lambda_k a_{ik} \right) = 0 \quad (8)$$

according to the Lagrange undetermined multiplier method with the elemental balance constraint

$$\sum_{i=1}^{N} n_i a_{ik} = A_k \quad (9)$$

Results and discussion

Catalyst characterization

Critical physico-chemical characteristics of Pd/SiO_2 and $Ba–Pd/SiO_2$ are given in Table 1. The SSA of Pd/SiO_2 was close to that of the SiO_2 support (200 $m^2 g^{-1}$). In contrast, $Ba–Pd/SiO_2$ exhibited a significantly lower SSA, which can be ascribed to partial pore blockage as observed for silica supported Pd/lanthanide bimetallics prepared from analogous precursors.[32] The TPR profile for Pd/SiO_2 (Fig. 2(I)) exhibited a negative peak (H_2 release) at 368 K that can be attributed to Pd hydride decomposition.[33] The profile for $Ba–Pd/SiO_2$ (Fig. 2(II)) is also characterized by H_2 release with T_{max} at 354 K and an associated Pd hydride composition (H/Pd ratio = 0.19) that differed from Pd/SiO_2 (0.34). The lower H/Pd suggests inhibited hydride formation due to the incorporation of Ba with the possible formation of smaller Pd particles as size governs hydride composition with an upper H/Pd = 0.76 for bulk Pd.[34] A shift in hydride decomposition temperature to a lower value also correlates with a decrease

Table 1 Physico-chemical properties of SiO_2-supported Pd and Ba–Pd catalysts

	Pd/SiO_2	$Ba–Pd/SiO_2$
SSA ($m^2 g^{-1}$)	191	154
TPR T_{max} (K)	368[a]	354[a], 573[b]
Pd hydride (H/Pd, mol mol^{-1})	0.34	0.19
H_2 chemisorption (μmol g^{-1})	7	46
H_2 TPD (μmol g^{-1})	19	91
NH_3 chemisorption (mmol g^{-1})	0.49	0.34
NH_3 TPD (mmol g^{-1})	0.48	0.32
d_{TEM} (nm)	28	7
d_c (nm)	33	9

[a] H_2 release.
[b] H_2 consumption.
TPD: temperature programmed desorption; TPR: temperature programmed reduction; SSA: specific surface area.

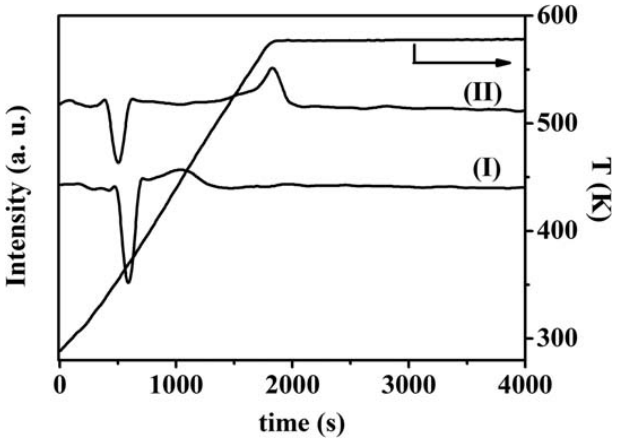

Figure 2 Temperature-programmed reduction (TPR) profiles for (I) Pd/SiO_2 and (II) $Ba-Pd/SiO_2$

in Pd particle size.[35] Hydrogen consumption at 573 K for $Ba-Pd/SiO_2$ suggests a temperature-induced reduction step, which may result from stabilization of surface Pd oxide with the addition of Ba.[27] Supported Pd morphology was determined by TEM analysis, and representative images (with associated size distributions) are presented in Fig. 3. Both catalysts display quasi-spherical Pd nano-particles with a narrower distribution of smaller particles for $Ba-Pd/SiO_2$ (mean size = 7 nm) compared with Pd/SiO_2 (28 nm). This result is in good agreement with Pd size obtained from application of the Scherrer equation to XRD line broadening (Table 1) and is inline with the work of Liu *et al.*[36] who observed an increase in metal dispersion for zeolite supported Pt following Ba exchange. The incorporation of Ba has been shown to minimize Pd agglomeration with the formation of smaller Pd particles.[27,37] Piacentini *et al.*[38] reported increased Pt dispersion at higher Ba loadings in $Ba-Pt/Al_2O_3$. Enhanced Pd dispersion can account for the greater H_2 chemisorption on $Ba-Pd/SiO_2$ relative to Pd/SiO_2 (Table 1), where smaller Pd particles facilitate dissociative H_2 adsorption.[39] Hydrogen release from both catalysts during TPD (Table 1) exceeded that adsorbed in ambient temperature pulse titration, diagnostic of spillover hydrogen during TPR.[40] Hydrogen TPD from Pd/SiO_2 generated the profile given in Fig. 4(I), characterized by a two-stage release with T_{max} = 775 and 1273 K (final isothermal hold). Drawing on available literature, the lower temperature peak can be ascribed to loss of chemisorbed hydrogen from Pd.[41] This is consistent with the equivalence of H_2 desorbed over 720–980 K (6 μmol g^{-1}) and that chemisorbed (Table 1). Hydrogen release at higher (1050–1273 K) temperatures has been attributed to desorption from the support and metal/support interface.[27,42] The TPD profile for $Ba-Pd/SiO_2$ (Fig. 4(II)) also showed two desorption peaks with a greater (by a factor of 5) amount of H_2 desorbed compared with Pd/SiO_2 (Table 1). This can be linked to the presence of smaller Pd particles that facilitate higher H_2 uptake and diffusion/spillover to the support.[43] The shift of the second H_2 desorption peak for $Ba-Pd/SiO_2$ to a lower temperature suggests that the incorporation of Ba impacts on spillover release.[27] Panagiotopoulou and Kondarides[44] recorded a displacement of H_2-TPD to a lower temperature (by 50 K) for Ca-promoted Pt/TiO_2 that they attributed to a modification of the metal-support interface with the formation of $Pt-Ca-Ti^{3+}$ sites that exhibit weaker Pt–H bond strength.

Surface acidity was probed by NH_3 chemisorption/desorption where TPD (Fig. 5*a*) from the silica support (I) exhibited NH_3 release with T_{max} = 343 K that can be attributed to weak acid sites.[45,46] Both Brønsted (hydroxyl groups acting as proton donors)[46] and weak Lewis acid sites[45,46] have been detected on silica surfaces by FTIR spectroscopy. Temperature programmed desorption from Pd/SiO_2 (II) and $Ba-Pd/SiO_2$ (III) exhibited a common T_{max} (= 357 K) with NH_3 desorption (0.15 mmol g^{-1}) close to that observed for SiO_2 (0.19 mmol g^{-1}). Integration of NH_3 desorption signals gave a total release that correlated well with the chemisorption measurements (Table 1). A secondary higher temperature (600–1000 K) NH_3 release was in evidence that must be linked to surface acidity generated during metal incorporation and sample treatment. Gao *et al.*[47] recorded an additional NH_3 desorption peak at 475–775 K for Ni/SiO_2 that was not observed for SiO_2. Moreover, Jiang *et al.*[48] reported an increase in NH_3 release at *ca.* 773 K during TPD of Pd/SBA with increasing Pd content (0.005 → 0.01 wt%) Ammonia chemisorption/desorption was lower for $Ba-Pd/SiO_2$ compared with Pd/SiO_2 (Table 1). X-ray diffraction analysis of $Ba-Pd/SiO_2$ (Fig. 5*b*) has revealed peaks characteristic of metallic Pd and a $BaSiO_3$ phase. The formation of $BaSiO_3$ can result in a consumption of surface acid sites. Labalme and co-workers[49] also reported a decrease in total surface acidity as a result of Ba addition to Pt/Al_2O_3 based on NH_3 TPD, which was attributed to neutralization of surface hydroxyl groups. X-ray photoelectron spectroscopy (XPS) analysis has established the formation of an electron-rich Pd phase in $Ba-Pd/SiO_2$.[27] This is consistent with Labalme's conclusion of electron donation from electro positive Ba to Pt on Al_2O_3[50,51] and is inline with reports, which have concluded that addition of Ba increases the electron density of Pd sites.[52,53]

Butyronitrile hydrogenation: thermodynamic considerations

A thermodynamic analysis of butyronitrile hydrogenation was performed to determine system behavior at equilibrium. Under thermodynamic control, the nitrile reactant was fully converted under the reaction conditions employed in this study. The calculated equilibrium selectivity as a function of reaction temperature is presented in Fig. 6 where it can be seen that the tertiary amine is the predominant product (S = 83–90%). Production of equivalent amounts of butylamine and dibutylamine as by-products is favored by increasing temperature. Preferential tertiary amine production indicates that there is no thermodynamic barrier for the coupled reduction and condensation steps shown in Fig. 1.

Butyronitrile hydrogenation: catalytic activity/selectivity (at 473 K)

Taking 473 K as a benchmark temperature, fractional butyronitrile conversion (X) was time invariant over Pd/SiO_2 (I) and $Ba-Pd/SiO_2$ (II) where the latter exhibited higher nitrile conversion (Fig. 7*a*). This is significant given the temporal decline in activity reported in liquid[4–7,9,54–56] and gas phase[10,11,18,20] nitrile hydrogenation over supported

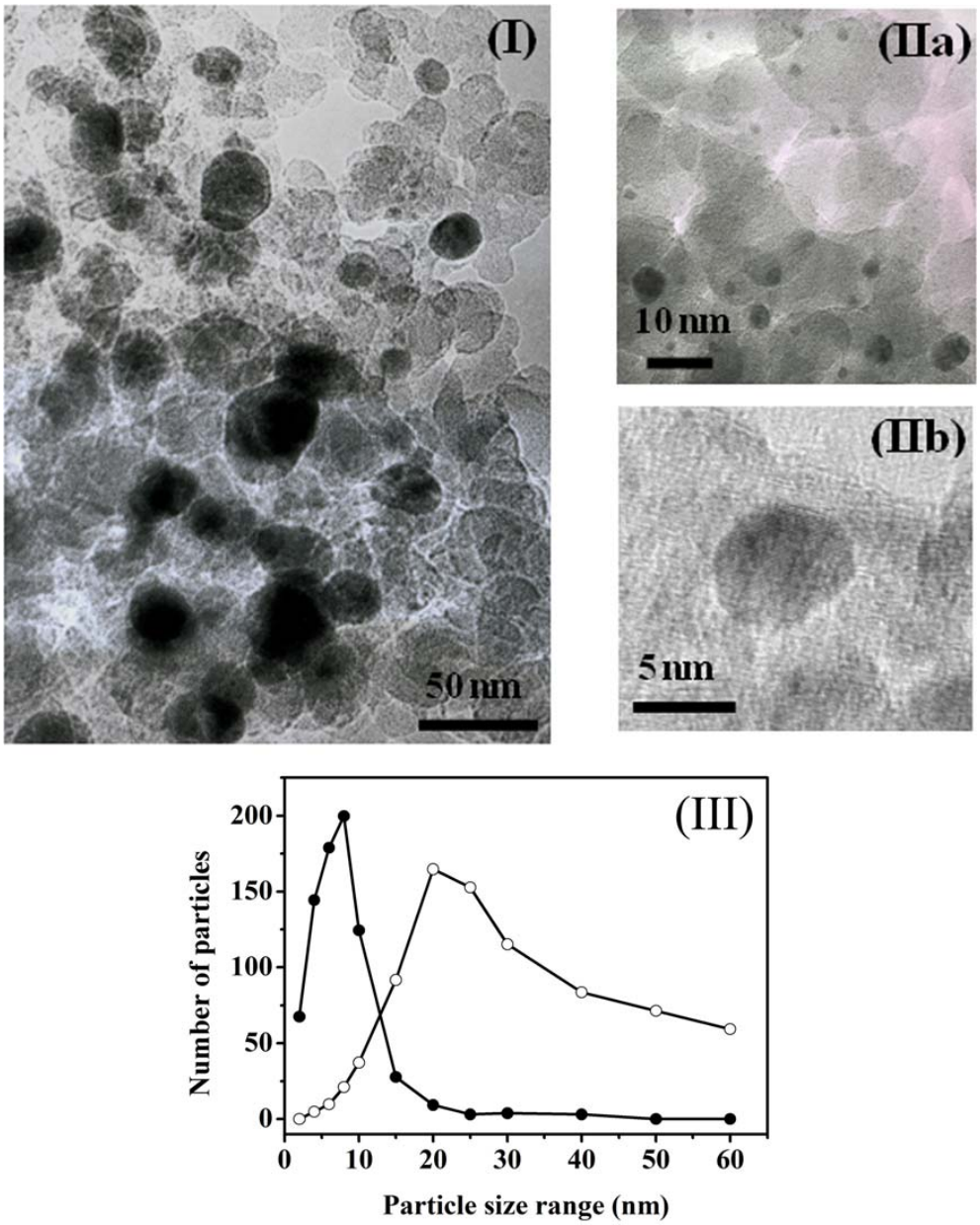

Figure 3 Representative transmission electron microscopy (TEM) images of (I) Pd/SiO_2 (○) and (II) $Ba–Pd/SiO_2$ (•) with (III) associated particle size distributions

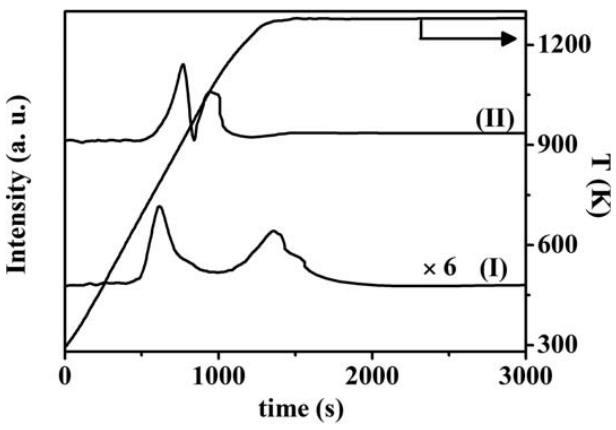

Figure 4 Hydrogen temperature-programmed desorption (TPD) profiles for (I) Pd/SiO_2 and (II) $Ba–Pd/SiO_2$

Pd,[5–7,9,55,56] Pt,[7,57] Ru,[7] and Ni.[11,19,20] Catalyst deactivation has been ascribed to metal particle agglomeration,[7,10] active site occlusion by amine product(s),[7,10,15,57,58] and catalyst coking associated with the formation of dehydrogenated surface species and carbides.[11,15,19,21] The greater levels of H_2 uptake/release exhibited by $Ba–Pd/SiO_2$ (Table 1) can account for the observed higher nitrile hydrogenation activity. Product distribution was invariant with conversion (Fig. 7*b* and *c*) where butylamine was the major product. This differs from predominant tertiary amine formation under thermodynamic equilibrium (Fig. 6) and demonstrates catalytic control. Nitrile transformation to amines via the pathways shown in Fig. 1 requires catalyst bifunctionality[59] where the metal phase serves to promote hydrogenation (steps (I), (II), (IV), and (VI)) and condensation of the imine intermediates with butyl- (step (III)) and dibutyl-amine

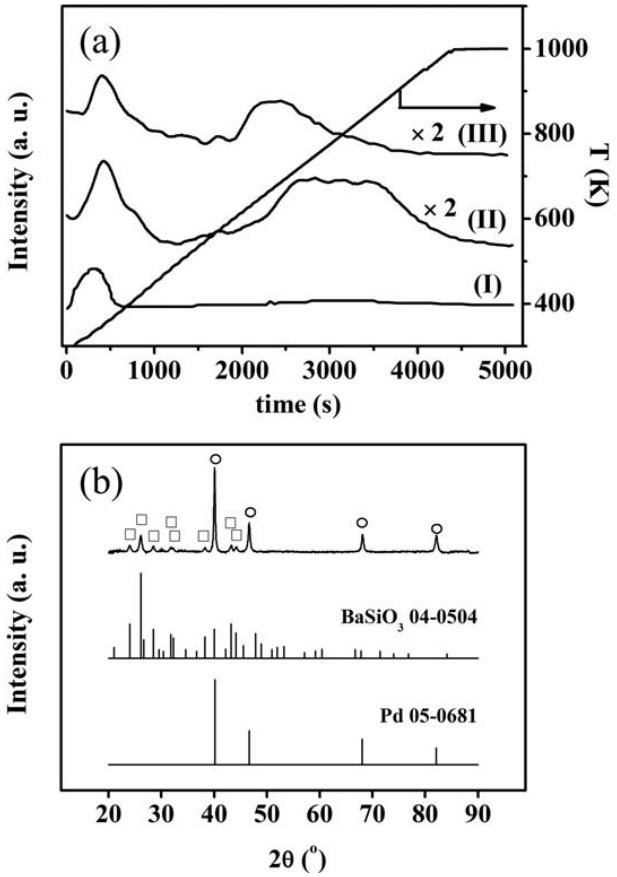

Figure 5 ***a*** **Ammonia temperature-programmed desorption (TPD) profiles for (I) SiO_2, (II) Pd/SiO_2, and (III) $Ba-Pd/SiO_2$;** ***b*** **X-ray diffraction (XRD) pattern for $Ba-Pd/SiO_2$ with peak assignments for Pd (○) and $BaSiO_3$ (□) phases. JCPDS-ICDD reference diffractograms for Pd (05-0681) and $BaSiO_3$ (04-0504) are also included**

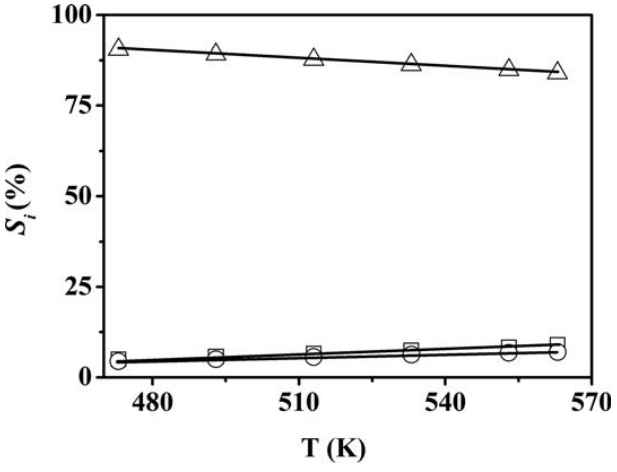

Figure 6 Product selectivity (S_i) as a function of reaction temperature at the thermodynamic equilibrium: butylamine (□); dibutylamine (○); tributylamine (Δ)

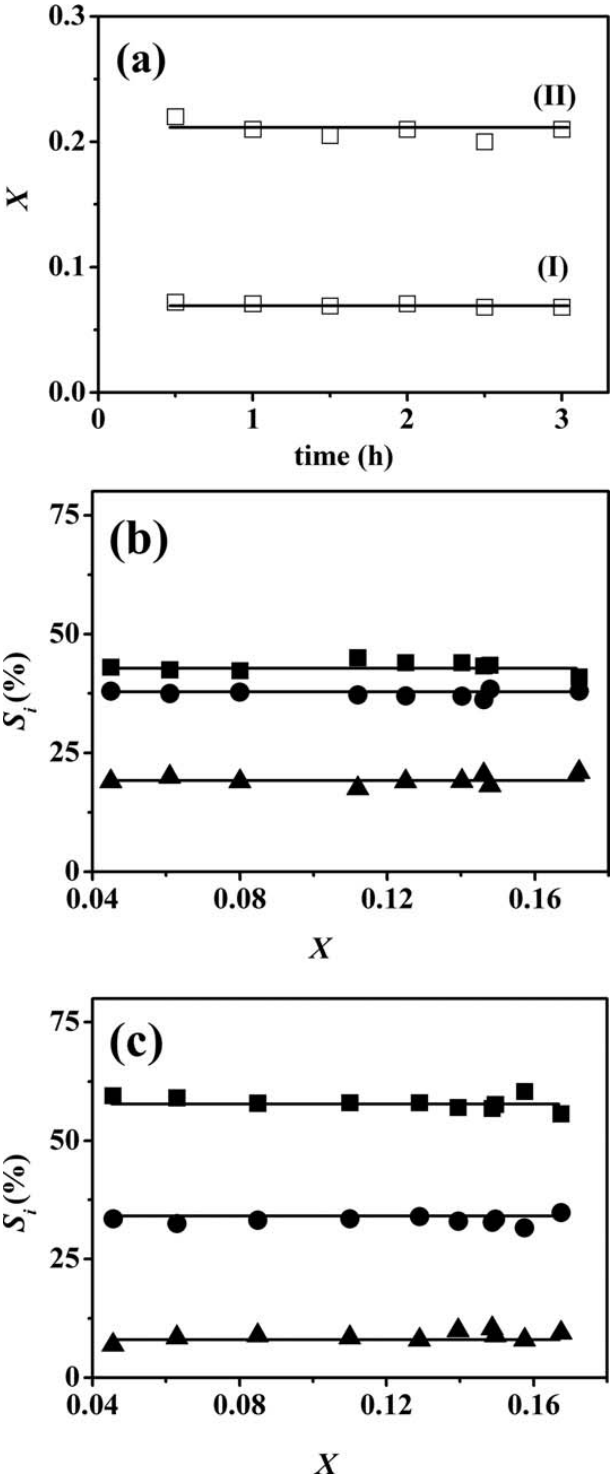

Figure 7 ***a*** **Time on-stream butyronitrile fractional conversion (*X*) for reaction over (I) Pd/SiO_2 and (II) $Ba-Pd/SiO_2$ and selectivity (S_i) to butylamine (■), dibutylamine (•), and tributylmine (▲) as a function of fractional conversion over** ***b*** **Pd/SiO_2 and** ***c*** **$Ba-Pd/SiO_2$;** ***Reaction conditions:*** ***P*** **= 1 atm, *T* = 473 K, $n/F = 3.4 \times 10^{-4}$–3.4×10^{-3} h**

(step (V)) proceeds on surface acid sites.[2,4,18,19,59] Selectivity to the target butylamine was higher over $Ba-Pd/SiO_2$ (Fig. 7*c*) than Pd/SiO_2 (Fig. 7*b*). This can be partly attributed to the lower surface acidity of the bimetallic catalyst that served to suppress condensation to secondary and tertiary amines. Moreover, weaker butylamine interaction with electron-rich Pd sites on $Ba-Pd/SiO_2$ resulting from repulsion with the $-NH_2$ function can favor desorption of the primary amine without further reaction. Branco *et al.*[24] reached a similar conclusion for the conversion of

propionitrile over lanthanide-promoted Cu where electron enriched Cu sites exhibited weaker adsorption of primary amine, limiting subsequent condensation.

Butyronitrile hydrogenation: temperature effects

Reaction temperature is a critical variable that impacts on reactant/intermediate activation and desorption dynamics, which in turn influence hydrogenation rate and product distribution.[60] The nitrile consumption rate delivered by Pd/SiO_2 (I) and $Ba-Pd/SiO_2$ (II) passed through maxima at 523 and 493 K, respectively, as shown in Fig. 8. Nieto-Márquez *et al.*[11] reported a maximum rate of butyronitrile hydrogenation over (carbon nanosphere) supported Ni at comparable temperatures ($463\ K < T < 583\ K$) that they linked to reactant thermal desorption that decreased surface coverage. Reaction over $Ba-Pd/SiO_2$ delivered higher nitrile consumption rates with the maximum at a lower temperature (493 K). The latter can be linked to weaker butyonitrile interaction via the nitrogen electron lone pair at electron rich Pd sites, resulting in more facile desorption. There is evidence in the literature[11] for a higher T_{max} in butyronitrile hydrogenation rate over Ni particles with lower electron density that can be attributed to stronger $-C \equiv N$ adsorption and the requirement for higher desorption temperatures. The higher selectivity to primary amine over $Ba-Pd/SiO_2$ (Fig. 8) can be ascribed to the lower surface acidity that limited condensation. Butylamine selectivity over both catalysts increased with increasing temperature to 100% at $T \geq 543\ K$. This is quite distinct from the thermodynamic equilibrium composition (Fig. 6) where tri-butylamine was the major product over the entire temperature range. An increase in temperature must induce desorption of the butylamine product, circumventing condensation. Cristiani and co-workers[61] have recorded an increase in primary amine formation ($S = 16-41\%$) at higher temperatures (453–563 K) in stearonitrile conversion over $CuO-Cr_2O_3$. In contrast, Braos-García and co-workers[21] noted decreasing primary amine selectivity and preferential secondary amine formation with increasing temperature (378–418 K) for acetonitrile hydrogenation over mixed alumina/gallium oxide (16% w/w Ga_2O_3) supported Ni. Nieto-Márquez *et al.*[11] have proposed that selectivity maxima are the result of contributions due to mass transfer, thermodynamic limitations, and thermal poisoning. The higher butyronitrile consumption rate delivered by $Ba-Pd/SiO_2$ coupled with reaction exclusivity translates into higher butylamine productivity ($91\ mol\ h^{-1}\ mol_{Pd}^{-1}$) than that achieved over Pd/SiO_2 ($54\ mol\ h^{-1}\ mol_{Pd}^{-1}$) at 543 K. Authors attribute this to greater availability of surface reactive hydrogen. It is important to note that in previous reports, reaction over Ni delivered higher activity and primary amine selectivity than Pd in liquid phase nitrile hydrogenation.[6,16] Authors have achieved an order of magnitude higher rate over $Ba-Pd/SiO_2$ with full selectivity to the target butylamine when compared with reported gas phase continuous reaction over supported Ni under similar reaction conditions ($T = 493\ K$, 1 atm).[10] Our results demonstrate that the combination of an alkaline earth metal (Ba) with Pd facilitates enhanced cleaner primary amine production.

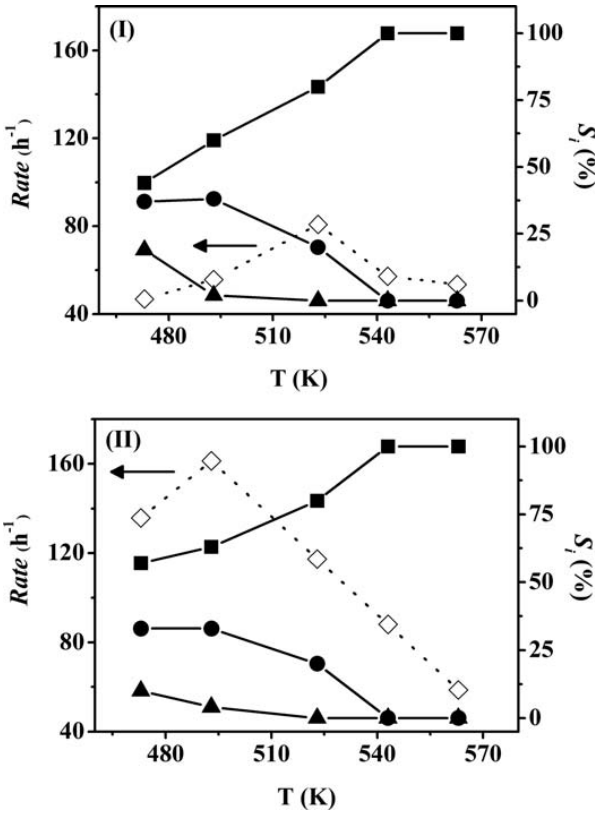

Figure 8 Reaction rate (◇, dashed lines) and selectivity (S_i, solid lines) to butylamine (■), dibutylamine (•), and tributylamine (▲) as a function of temperature for reaction over (I) Pd/SiO_2 and (II) $Ba-Pd/SiO_2$; *Reaction conditions:* $P = 1$ atm, $n/F = 1.4 \times 10^{-3}$ h

Conclusions

Authors have attained a higher selective butyronitrile hydrogenation rate ($91\ mol\ h^{-1}\ mol_{Pd}^{-1}$) to the target butylamine in the gas phase hydrogenation of butyronitrile over $Ba-Pd/SiO_2$ relative to Pd/SiO_2 ($54\ mol\ h^{-1}\ mol_{Pd}^{-1}$). The increased rate can be attributed to greater available surface reactive hydrogen (from H_2 chemisorption coupled with TPD) on $Ba-Pd/SiO_2$ bearing smaller metal nanoparticles (7 vs 28 nm). Lower surface acidity (from NH_3 adsorption/TPD) served to minimize side condensation and the formation of higher amines over $Ba-Pd/SiO_2$. Temperature-related activity maxima (T_{max}) are attributed to thermal desorption that limits surface coverage by reactant where T_{max} for $Ba-Pd/SiO_2$ (493 K) was lower than Pd/SiO_2 (523 K) reflecting weaker surface interaction for the former. Authors have provided the first reported evidence for (i) full selectivity to primary amine in nitrile hydrogenation over supported Pd; (ii) enhanced selective hydrogenation rate for a Pd-alkaline earth metal formulation that was 10 times higher than that reported previously for supported Ni.

Acknowledgment

Authors acknowledge the contribution of Prof. S. G. Shore and Dr X. Wang to this work and financial support to Y. Hao and M. Li through the Overseas Research Students Award Scheme (ORSAS).

References

1. J. Krupka and J. Pasek: *Curr. Org. Chem.*, 2012, **16**, (8), 988–1004.
2. S. Gómez, J. A. Peters and T. Maschmeyer: *Adv. Synth. Catal.*, 2002, **344**, (10), 1037–1057.

3. S. Nishimura: 'Handbook of heterogeneous catalytic hydrogenation for organic synthesis', 265–265; 2001, New York, John Wiley.
4. H. Chen, M. Xue, S. Hu and J. Shen: *Chem. Eng. J.*, 2012, **181–182**, (1), 677–684.
5. Y. Huang and W. M. H. Sachtler: *Appl. Catal. A Gen.*, 1999, **182**, (2), 365–378.
6. Y. Huang and W. M. H. Sachtler: *J. Catal.*, 1999, **188**, (1), 215–225.
7. Y. Huang, V. Adeeva and W. M. H. Sachtler: *Appl. Catal. A Gen.*, 2000, **196**, (1), 73–85.
8. P. Schärringer, T. E. Müller and J. A. Lercher: *J. Catal.*, 2008, **253**, (1), 167–179.
9. Y. Y. Huang and W. M. H. Sachtler: *J. Catal.*, 1999, **184**, (1), 247–261.
10. A. Nieto-Márquez, D. Toledano, P. Sánchez, A. Romero and J. L. Valverde: *J. Catal.*, 2010, **269**, (1), 242–251.
11. A. Nieto-Márquez, D. Toledano, J. C. Lazo, A. Romero and J. L. Valverde: *Appl. Catal. A Gen.*, 2010, **373**, (1–2), 192–200.
12. H. Chen, M. W. Xue and J. Y. Shen: *Catal. Lett.*, 2010, **135**, (3–4), 246–255.
13. A. Chojecki, M. Veprek-Heijman, T. E. Müller, P. Schärringer, S. Veprek and J. A. Lercher: *J. Catal.*, 2007, **245**, (1), 237–248.
14. D. J. Segobia, A. F. Trasarti and C. R. Apesteguía: *Appl. Catal. A Gen.*, 2015, **494**, (1), 41–47.
15. M. C. Carrión, B. R. Manzano, F. A. Jalón, I. Fuentes-Perujo, P. Maireles-Torres, E. Rodríguez-Castellón and A. Jiménez-López: *Appl. Catal. A Gen.*, 2005, **288**, (1–2), 34–42.
16. D. J. Segobia, A. F. Trasarti and C. R. Apesteguía: *Appl. Catal. A Gen.*, 2012, **445-446**, (1), 69–75.
17. C. Jiménez-González, P. Poechlauer, Q. B. Broxterman, B.-S. Yang, D. Am Ende, J. Baird, C. Bertsch, R. E. Hannah, P. Dell'Orco, H. Noorrnan, S. Yee, R. Reintjens, A. V. Massonneau and J. Manley: *Org. Process Res. Dev.*, 2011, **15**, (4), 900–911.
18. A. C. Gluhoi, P. Mărginean and U. Stănescu: *Appl. Catal. A Gen.*, 2005, **294**, (2), 208–214.
19. P. Braos-García, P. Maireles-Torres, E. Rodríguez-Castellón and A. Jiménez-López: *J. Mol. Catal. A Chem.*, 2003, **193**, (1–2), 185–196.
20. A. Nieto-Márquez, V. Jiménez, A. M. Raboso, S. Gil, A. Romero and J. L. Valverde: *Appl. Catal. A Gen.*, 2011, **393**, (1–2), 78–87.
21. P. Braos-García, P. Maireles-Torres, E. Rodríguez-Castellón and A. Jiménez-López: *J. Mol. Catal. A Chem.*, 2001, **168**, (1–2), 279–287.
22. N. Iwasa, M. Yoshikawa and M. Arai: *Phys. Chem. Chem. Phys.*, 2002, **4**, (21), 5414–5420.
23. M. Arai, T. Ebina and M. Shirai: *Appl. Surf. Sci.*, 1999, **148**, (3–4), 155–163.
24. J. B. Branco, D. Ballivet-Tkatchenko and A. P. de Matos: *J. Phys. Chem. C.*, 2007, **111**, (41), 15084–15088.
25. M. Armbrüster, M. Behrens, F. Cinquini, K. Föttinger, Y. Grin, A. Haghofer, B. Klötzer, A. Knop-Gericke, H. Lorenz, A. Ota, S. Penner, J. Prinz, C. Rameshan, Z. Révay, D. Rosenthal, N. Rupprechter, P. Sautet, R. Schlögl, L. Shao, L. Szentmiklósi, D. Teschner, D. Torres, R. Wagner, R. Widmer and G. Wowsnick: *ChemCatChem.*, 2012, **4**, (8), 1048–1063.
26. I. Favier, D. Madec, E. Teuma and M. Gómez: *Curr. Org. Chem.*, 2011, **15**, (18), 3127–3174.
27. E. Ding, S. Jujjuri, M. Sturgeon, S. G. Shore and M. A. Keane: *J. Mol. Catal. A Chem.*, 2008, **294**, (1–2), 51–60.
28. D. W. Knoeppel, J. P. Liu, E. A. Meyers and S. G. Shore: *Inorg. Chem.*, 1998, **37**, (19), 4828–4837.
29. A. L. Bugaev, A. A. Guda, K. A. Lomachenko, V. V. Srabionyan, L. A. Bugaev, A. V. Soldatov, C. Lamberti, V. P. Dmitriev and J. A. van Bokhoven: *J. Phys. Chem. C.*, 2014, **118**, (19), 10416–10423.
30. U. Holzwarth and N. Gibson: *Nat. Nanotechnol.*, 2011, **6**, (9), 534–534.
31. X. Wang, S. Li, H. Wang, B. Liu and X. Ma: *Energy Fuel.*, 2008, **22**, (6), 4285–4291.
32. S. Jujjuri, E. Ding, S. G. Shore and M. A. Keane: *J. Mol. Catal. A Chem.*, 2007, **272**, (1–2), 96–107.
33. F. Menegazzo, T. Fantinel, M. Signoretto and F. Pinna: *Catal. Commun.*, 2007, **8**, (6), 876–879.
34. F. Cárdenas-Lizana, Y. Hao, M. Crespo-Quesada, I. Yuranov, X. Wang, M. A. Keane and L. Kiwi-Minsker: *ACS Catal.*, 2013, **3**, (6), 1386–1396.
35. S. Gómez-Quero, F. C. árdenas-Lizana and M. A. Keane: *Ind. Eng. Chem. Res.*, 2008, **47**, (18), 6841–6853.
36. P. Liu, X. Zhang, Y. Yao and J. Wang: *React. Kinet. Mech. Catal.*, 2010, **100**, (1), 217–226.
37. F. Klingstedt, H. Karhu, A. K. Neyestanaki, L. E. Lindfors, T. Salmi and J. Väyrynen: *J. Catal.*, 2002, **206**, (2), 248–262.
38. M. Piacentini, R. Strobel, M. Maciejewski, S. E. Pratsinis and A. Baiker: *J. Catal.*, 2006, **243**, (1), 43–56.
39. A. M. Doyle, S. K. Shaikhutdinov, S. D. Jackson and H.-J. Freund: *Angew. Chem. Int. Ed. Engl.*, 2003, **42**, (42), 5240–5243.
40. C. Tu and S. Cheng: *ACS Sust. Chem. Eng.*, 2013, **2**, (4), 629–636.
41. C. Amorim, G. Yuan, P. M. Patterson and M. A. Keane: *J. Catal.*, 2005, **234**, (2), 268–281.
42. M. Chettibi, A.-G. Boudjahem and M. Bettahar: *Trans. Met. Chem.*, 2011, **36**, (2), 163–169.
43. S. D. Lin and M. A. Vannice: *J. Catal.*, 1993, **143**, (2), 563–572.
44. P. Panagiotopoulou and D. I. Kondarides: *Appl. Catal. B Environ.*, 2011, **101**, (3), 738–746.
45. A. V. Biradar, S. B. Umbarkar and M. K. Dongare: *Appl. Catal. A Gen.*, 2005, **285**, (1–2), 190–195.
46. L. Óvári and F. Solymosi: *J. Mol. Catal. A Chem.*, 2004, **207**, (1), 35–40.
47. C.-G. Gao, Y.-X. Zhao and D.-S. Liu: *Catal. Lett.*, 2007, **118**, (1–2), 50–54.
48. J. Jiang, C. Yang, J. Sun, T. Li and F. Cao: *Adv. Chem. Eng. Res.*, 2013, **2**, (4), 73–78.
49. V. Labalme, B. Béguin, F. Gaillard and M. Primet: *Appl. Catal. A Gen.*, 2000, **192**, (2), 307–316.
50. V. Labalme, E. Garbowski, N. Guilhaume and M. Primet: *Appl. Catal. A Gen.*, 1996, **138**, (1), 93–108.
51. V. Labalme, N. Benhamou, N. Guilhaume, E. Garbowski and M. Primet: *Appl. Catal. A Gen.*, 1995, **133**, (2), 351–366.
52. N. Mahata, K. V. Raghavan, V. Vishwanathan and M. A. Keane: *React. Kinet. Catal. Lett.*, 2001, **72**, (2), 297–302.
53. K. Tanikawa and C. Egawa: *Appl. Catal. A Gen.*, 2011, **403**, (1–2), 12–17.
54. P. Kukula and K. Koprivova: *J. Catal.*, 2005, **234**, (1), 161–171.
55. L. Hegedűs, T. Máthé and T. Kárpáti: *Appl. Catal. A Gen.*, 2008, **349**, (1–2), 40–45.
56. L. Hegedűs and T. Máthé: *Appl. Catal. A Gen.*, 2005, **296**, (2), 209–215.
57. M. Arai, Y. Takada and Y. Nishiyama: *J. Phys. Chem. B.*, 1998, **102**, (11), 1968–1973.
58. P. F. Yang, Z. X. Jiang, P. L. Ying and C. Li: *J. Catal.*, 2008, **253**, (1), 66–73.
59. M. J. F. M. Verhaak, A. J. van Dillen and J. W. Geus: *Catal. Lett.*, 1994, **26**, (1–2), 37–53.
60. M. P. González-Marcos, J. I. Gutiérrez-Ortiz, C. González-Ortiz De Elguea, J. I. Alvarez and J. R. González-Velasco: *Can. J. Chem. Eng.*, 1998, **76**, (5), 927–935.
61. C. Cristiani, G. Groppi, G. Airoldi and P. Forzatti: 'Catalytic hydrogenation', in 'Studies in surface science and catalysis', Eds. K. K. Unger, G. Kreysa and J. P. Baselt, 128–128; 1986, Amsterdam, Elesvier Science Publishers.